GEOLOGY | THE GEOLOGICAL SOCIETY OF AMERICA®

https://doi.org/10.1130/G52558.1

Manuscript received 8 July 2024
Revised manuscript received 23 October 2024
Manuscript accepted 5 November 2024

Published online 20 November 2024

Real-time, in situ viscosity mapping of active lava

M.A. Harris[1,*], M.O. Chevrel[1,2,3,4], J.T. Parsons[1], T. Latchimy[2], T. Thordarson[5], A. Höskuldsson[6], W.M. Moreland[5], M. Payet–Clerc[3,5], and S. Kolzenburg[1]

[1]Department of Geology, State University of New York at Buffalo, 126 Cooke Hall Buffalo, New York 14260-4130, USA
[2]Université Clermont Auvergne, CNRS, IRD, OPGC, Laboratoire Magmas et Volcans, F-63000 Clermont-Ferrand, France
[3]Université Paris Cité, Institut de Physique du Globe de Paris, CNRS, 75005 Paris, France
[4]Observatoire Volcanologique du Piton de la Fournaise, Institut de Physique du Globe de Paris, 97418 La Plaine des Cafres, France
[5]Faculty of Earth Sciences, University of Iceland, Sturlugata 7, IS-102 Reykjavík, Iceland
[6]Nordic Volcanological Centre, Institute of Earth Sciences, University of Iceland, Sturlugata 7, IS-102 Reykjavík, Iceland

ABSTRACT

Viscosity is a fundamental physical property that controls lava flow dynamics, runout distance, and velocity, which are critical factors in assessing and mitigating risks associated with effusive eruptions. Natural lava viscosity is driven by a dynamic interplay among melt, crystals, and bubbles in response to the emplacement conditions. These conditions are challenging to replicate in laboratory experiments, yet this remains the most common method for quantifying lava rheology. Few in situ viscosity measurements exist, but none of those constrains the spatial evolution of viscosity along an entire active lava flow field. Here, we present the first real-time, in situ viscosity map of active lava as measured in the field at Litli-Hrútur, Iceland. We precisely measured a lava viscosity increase of over two orders of magnitude, associated with a temperature decrease, crystallinity increase, and vesicularity decrease from near-vent to distal locations, crossing the pāhoehoe–'a'ā transition. Our data expand the limited database of three-phase lava viscosity, which is crucial for improvements and validation of the current numerical, experimental, and petrological approaches used to estimate lava viscosity. Further, this study showcases that field viscometry provides a rapid, accurate, and precise assessment of lava viscosity that can be implemented in eruptive response modeling of lava transport.

INTRODUCTION

Eruptive style, flow velocity, morphology, and runout distance are controlled by viscosity. Viscosity parameterizations have largely been derived from analog materials and remelted rocks in the laboratory (Mader et al., 2013; Kolzenburg et al., 2022). Laboratory experiments allow for precise control of temperature, shear rate, and oxygen fugacity, but they struggle to reproduce the three-phase nature (melt + crystals + bubbles) of lava, as they usually lack a gas phase. Viscosity determinations of active lava have proven effective at capturing bulk properties, but the methods rely on observations of channelized lavas and quantification of the flow rate (e.g., Moore, 1987; Fink and Zimbelman, 1990; Lev and James, 2014). Note that any measurement of three-phase suspensions represents a single point of apparent viscosity along the materials flow curve, but we use the term viscosity in this manuscript for brevity.

Viscosity data are used in lava flow models to aid the forecasting of flow paths and runouts (Harris and Rowland, 2001; Costa and Macedonio, 2005; Cappello et al., 2016; Hyman et al., 2022). Rapid viscosity determinations have been sought after for decades, and current approaches like channel velocity estimates and petrographic modeling have been applied for recent eruptions (e.g., Kīlauea—Dietterich et al., 2021; Cumbre Vieja—Pankhurst et al., 2022; Piton de la Fournaise—Chevrel et al., 2022). However, if channel geometry, topography, and effusion rate assumptions are used for viscosity determinations, their uncertainties propagate to the predicted flow paths. Additionally, petrographic methods require at least several days to process the lava texture and chemistry needed for the viscosity estimate.

Alternatively, in situ viscosity measurements of lava provide a direct value and yield detailed information on the dynamic, three-phase lava viscosity (Chevrel et al., 2018a). To date, in situ measurements have been decoupled from laboratory studies and scarcely implemented at isolated locations (Chevrel et al., 2019). This is largely due to a lack of portable and accurate measurement devices. Recent advances have provided two new portable field viscometers: a motor-driven rotational viscometer (RV) by Chevrel et al. (2023) for low viscosities (10^1–10^3 Pa·s), and a lava penetrometer (LP) by Harris et al. (2024) for medium to high viscosities (10^3–10^5 Pa·s).

Here, using these devices, we present the first set of in situ viscosity measurements that cover an entire active lava flow. Measurements were performed at the Litli-Hrútur eruption on the Reykjanes Peninsula, Iceland (Fig. 1). The mean output rate was 4 ± 2 m^3/s with an eruptive volume of 12×10^6 m^3 dense rock equivalent (Thordarson et al., 2023). The composition of the erupted lava is tholeiitic basalt (see Item S1 in the Supplemental Material[1]) with porphyritic plagioclase (15%–25%) and minor olivine (2%–5%) phenocrysts. Our measurements provide unprecedented viscosity data associated with decreasing temperature and vesicularity

M.A. Harris https://orcid.org/0000-0001-8905-3026
*martin.a.harris95@gmail.com

[1]Supplemental Material. Item S1: Major-element and glass chemistry of Litli-Hrútur samples, methods, and data tables. Item S2: Combined in situ viscosity and temperature for all measurements conducted in Litli-Hrútur lavas, text, glass thermometry data figure, and data table. Item S3: Calibration for the rotational viscometer, and description of the procedure with a corresponding figure. Item S4: Photomicrographs and textures of Litli-Hrútur samples, methods, and representative figures of lava textures. Item S5: Petrologic approach to modeling three-phase Litli-Hrútur lavas, and data table. Please visit https://doi.org/10.1130/GEOL.S.27616911 to access the supplemental material; contact editing@geosociety.org with any questions.

CITATION: Harris, M.A., et al., 2024, Real-time, in situ viscosity mapping of active lava: Geology, v. XX, p. , https://doi.org/10.1130/G52558.1

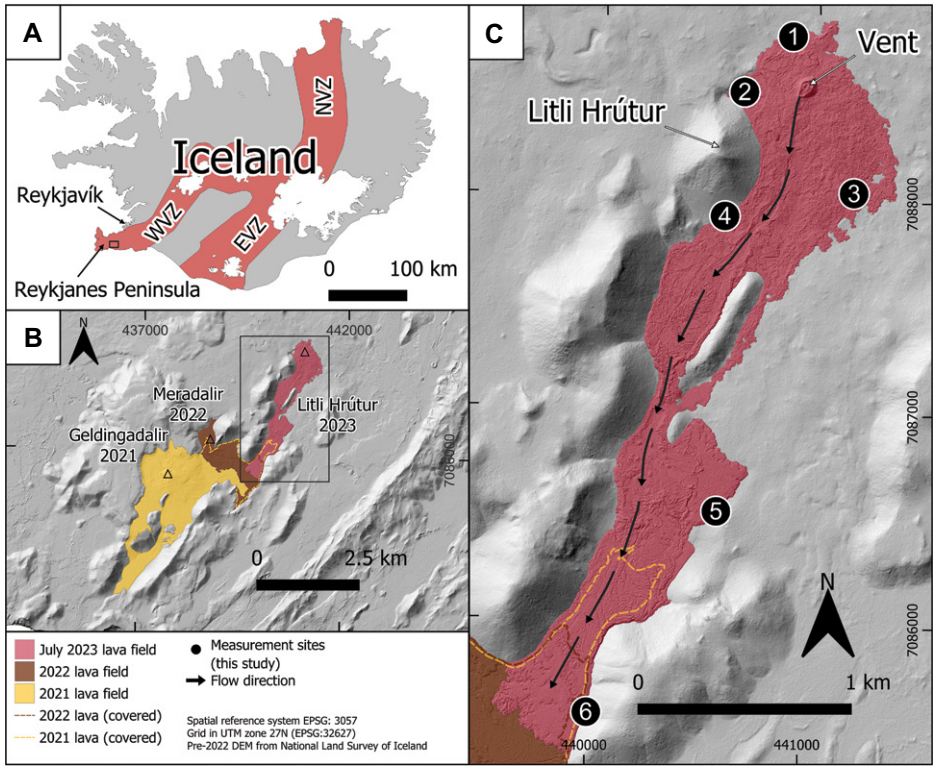

Figure 1. Location of measurement sites on lava flow field of 2023 Litli-Hrútur, Iceland, eruption. (A) Regional setting of eruption site within southwest Reykjanes Peninsula. Black rectangle denotes part B location. Rift zones (red) and ice caps (white) are shown. (B) Map showing extent of 2021, 2022, and 2023 lava flow fields in area. Triangles denote approximate vent locations. Black rectangle denotes part C location. Rift zones (red), North, East, and West Volcanic Zones (NVZ, EVZ, WVZ, respectively), and ice caps (white) are shown. (C) Map showing extent of lava flow field with six measurement site locations. UTM—Universal Transverse Mercator; EPSG—European Petroleum Survey Group; DEM—digital elevation model.

and increasing crystallinity along the flow, including a constraint over the pāhoehoe–ʻaʻā transition.

This study showcases the potential for in situ measurements to record detailed three-phase lava rheology at significantly faster time scales than currently used methods. Such data can be used to improve or validate current understanding of multiphase lava rheology. Rapid and precise field viscometry, as done here for the first time for an entire flow field, can also promote enhanced real-time models of lava flow propagation used in civil protection efforts.

METHODS

We conducted viscosity measurements at six locations (Fig. 1C) from 17 to 26 July starting seven days after the eruption onset (see Item S2). The lava flowed on a flat-lying valley, in a channel that transitioned from pāhoehoe to ʻaʻā after ~2 km. The channel was inaccessible, but repeated partial collapse of the vent led to channel overflows and breakouts that made lava accessible for measurements. The sample collected 250 m from the vent, at site 1, is consistent with the textural and chemical properties of vent spatters (Krmíček et al., 2023), and we documented the three-phase textural and thermal evolution of all remaining sites down to the flow front at 3200 m from the vent (Table 1). As a result, we consider the textural and thermal properties of the measured lavas to be representative of lava during flow in the entire system.

RV measurements were performed at sites 1 and 3, in breakout pāhoehoe lobes. They recorded the torque of a rotating shear vane immersed in the lava for 1 to 3 min (Fig. 2A). LP measurements were performed at sites 2, 3, 4, 5, and 6, in pāhoehoe lobes and windows of accessible ʻaʻā lava at the flow front. They recorded the force required to push a hemispherical indenter into the lava over ~20 cm and a duration of ~2–15 s (Fig. 2C). Both devices are open-source devices; specifications and calibration to directly recover viscosity are presented in Chevrel et al. (2023), in Harris et al. (2024), and in Item S3.

Lava temperatures were measured at each site using K-type thermocouples immersed at ~10–20 cm depth for 2–3 min (Fig. 2F), and measurements with a stable reading over ~50 s were deemed to be valid. Samples were collected at each site (Figs. 2B and 2E) and quenched in water to suppress further crystallization and maintain the textures of the lava while flowing. Representative material was used to quantify crystals and vesicles (area %) (Item S4). We used Thermobar (Wieser et al., 2022) to calculate pressures and water-independent glass temperatures from electron microprobe–derived glass MgO analyses for each site (Fig. 3; Items S1 and S2).

RESULTS

The lava morphology transitioned over a distance of 3200 m from sheet and slabby pāhoehoe (sites 1–3) near the vent to transitional spiney pāhoehoe (site 4) to rubbly ʻaʻā (site 5), and blocky ʻaʻā (site 6) in the distal sectors of the

TABLE 1. SUMMARY OF VISCOSITY AND TEMPERATURE MEASUREMENTS AND SAMPLE TEXTURES FOR EACH SITE, LITLI-HRÚTUR ERUPTION, ICELAND

Site no.	UTM E	UTM N	Measurement type	Viscosity (Pa•s)	2σ	Temperature (°C)	Crystal %	2σ	Bubble %	2σ	Distance from vent (m)
1	440846	7088729	Rotational[80]	322	77	1165	25	1	32	5	250
2	440626	7088462	Penetrometer	399	48	1164	30	2	15	5	370
3*	441154	7087999	Rotational[80]	2521	85	1161	27	4	20	11	650
3*	441154	7087999	Rotational[30]	3270	1548	1161	27	4	20	11	650
3*	441154	7087999	Penetrometer	643	155	1161	27	4	20	11	650
3†	441154	7087999	Rotational[30]	3571	456	1162	–	–	17	6	650
3†	440551	7087877	Rotational[60]	2008	614	1162	–	–	17	6	650
4	440551	7087877	Penetrometer	1302	304	1163	33	3	12	6	900
5	440625	7086421	Penetrometer	5311	913	1155§	47	2	12	6	2400
6	439971	7085528	Penetrometer	19,439	1355	1150	51	5	2	1	3200
6	439971	7085528	Penetrometer	37,679	4563	1148	51	5	2	1	3200
6	439971	7085528	Penetrometer	13,963	1480	1152	51	5	2	1	3200

Notes: Coordinate system: Universal Transverse Mercator (UTM) Zone 27N; European Petroleum Survey Group (EPSG) 32627. Rotational shear vane sizes: [80] = 80 × 25 mm; [60] = 60 × 20 mm; [30] = 30 × 15 mm.
*Measurements conducted at site 3 on 25 July 2023.
†Measurements conducted at site 3 on 26 July 2023.
§Obtained from corrected glass temperature.

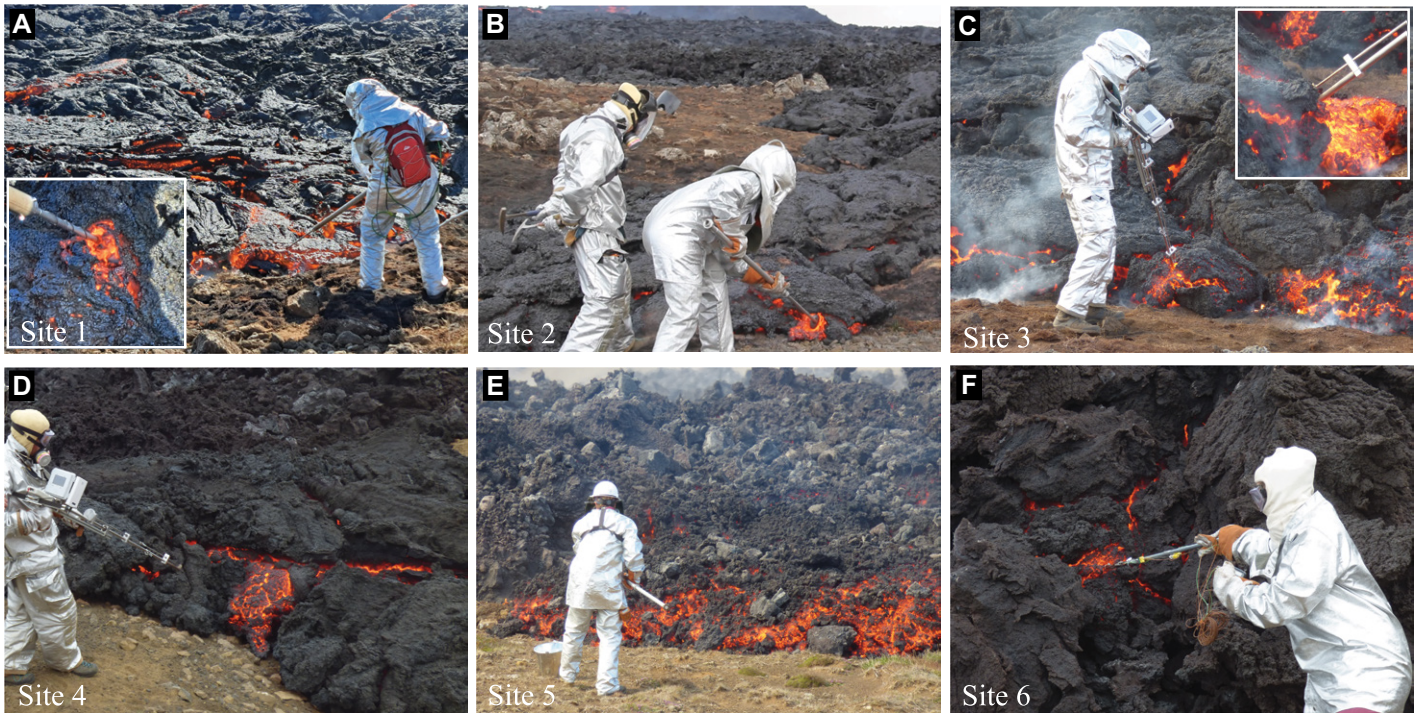

Figure 2. Field photos of six sites where viscosity and temperature measurements as well as sampling were performed. (A) Site 1, using rotational viscometer within sheet pāhoehoe lavas. (B) Site 2, sampling of spiny pāhoehoe lavas. (C) Site 3, using lava penetrometer within spiny pāhoehoe lavas. (D) Site 4, using lava penetrometer within transitional spiny pāhoehoe lavas. (E) Site 5, sampling lava on rubbly 'a'ā flow front. (F) Site 6, performing temperature measurement on 'a'ā lava flow front.

flow field (Fig. 2; Table 1). We recorded in situ temperatures for five of the six sites, logging a decrease of lava temperature from 1165 °C to 1148 °C over a distance of 3.2 km, equating to a cooling rate of 4.9 °C/km (Fig. 3A). The calculated glass temperatures systematically underestimated the lava temperatures by ~5 °C compared with in situ measurements, although the cooling rate remains similar (4.1 °C/km). We measured an increase in viscosity, from 322 Pa·s near the vent to 37,770 Pa·s at the flow front (Figs. 3C and 3D; Table 1; Item S2). Lava groundmass crystallinity along the path increased from 25% to 51%, and vesicularity decreased from 32% to 2% (Fig. 3B; Table 1; Item S2).

At site 3, where both field rheometers were used, we recovered in situ viscosities that spanned 643 Pa·s (LP) to 2000–3500 Pa·s (RV). This variation is explained by the thermal gradients within the lavas. The LP viscosities were measured at depths of ~10–15 cm within the lava (Harris et al., 2024), where the independent thermocouple measurements were recorded, whereas the depths for RV measurements were closer to the surface, within ~5–10 cm. Thus, the LP data represent the hotter interior, and the RV data represent cooler crust, potentially entering the viscoelastic regime (Pinkerton and Sparks, 1978; James et al., 2004). In situ techniques can therefore quantify the change in the viscosity of the viscous horizon along the outer boundary of the lava (Belousov and Belousova, 2018), which excerpts the most significant control on the flow at active lava fronts and margins.

DISCUSSION

Temperature, Viscosity, and Textural Evolution of Lavas

Since the composition of the Litli-Hrútur lavas did not change within the flow field (Item S1), any change in viscosity along the ~3 km (Fig. 3) flow was the result of thermal and textural changes within the lava. Prior work on suspension rheology has shown that increasing the particle fraction of a suspension toward the maximum packing fraction (~50%–70%) causes an exponential increase in effective viscosity due to particle jamming, followed by flattening of effective viscosity at very high particle fractions (Costa et al., 2009). Additionally, the bubble fraction within a suspension has been shown to decrease the effective viscosity when the capillary number (Ca) >1, where bubbles deform, and to increase effective viscosity when Ca <1, when bubbles act as rigid solids (Mader et al., 2013).

The pāhoehoe–'a'ā transition is driven by cooling and crystallization, by increasing lava viscosity (Cashman et al., 1999; Robert et al., 2014; Di Fiore et al., 2021), or by increasing effusion rate or steepening of the flow path, causing higher strain rates (Keszthelyi et al., 2004; Guilbaud et al., 2005). The Litli-Hrútur effusion rate remained steady throughout all field measurements, and lavas spread across a flat valley with no drastic slope changes; therefore, changes in strain rate will not have contributed to the pāhoehoe–'a'ā transition of the Litli-Hrútur lavas, which took place between sites 4 and 5 (Fig. 3C). While vesicularity remained steady between these sites, crystallinity increased from 33% to 47%, temperature decreased from 1163 °C to 1155 °C, and viscosity changed from 1302 ± 304 Pa·s to 5311 ± 913 Pa·s. This data set represents the first in situ measurements that constrain the pāhoehoe–'a'ā transition zone in active lava (Fig. 3; Table 1). This transition has previously been investigated through morphological, petrological, and experimental studies, which proposed that the transition takes place between 500 and 10^5 Pa·s at low shear rates (<2 s^{-1}) (Hon et al., 2003; Robert et al., 2014; Di Fiore et al., 2021), which broadly agree with our in situ data.

The Ca of bubbles in all samples was >3 (Item S5), and thus bubbles acted to decrease the effective viscosity. This is supported by site 1 pāhoehoe measurements (vesicularity >30%), which recorded viscosities that were >300% lower than measurements at site 4 pāhoehoe (vesicularity 12%) (Table 1). We found that while crystallinity increased across the pāhoehoe–'a'ā transition (~14%), the vesicularity change was minimal (~1%; Fig. 3B). In contrast, the final large viscosity increase (~5300–37,000 Pa·s) from the rubbly 'a'ā to blocky 'a'ā front (sites 5–6) is attributed to a moderate crystallinity increase (~4%) approaching the maximum

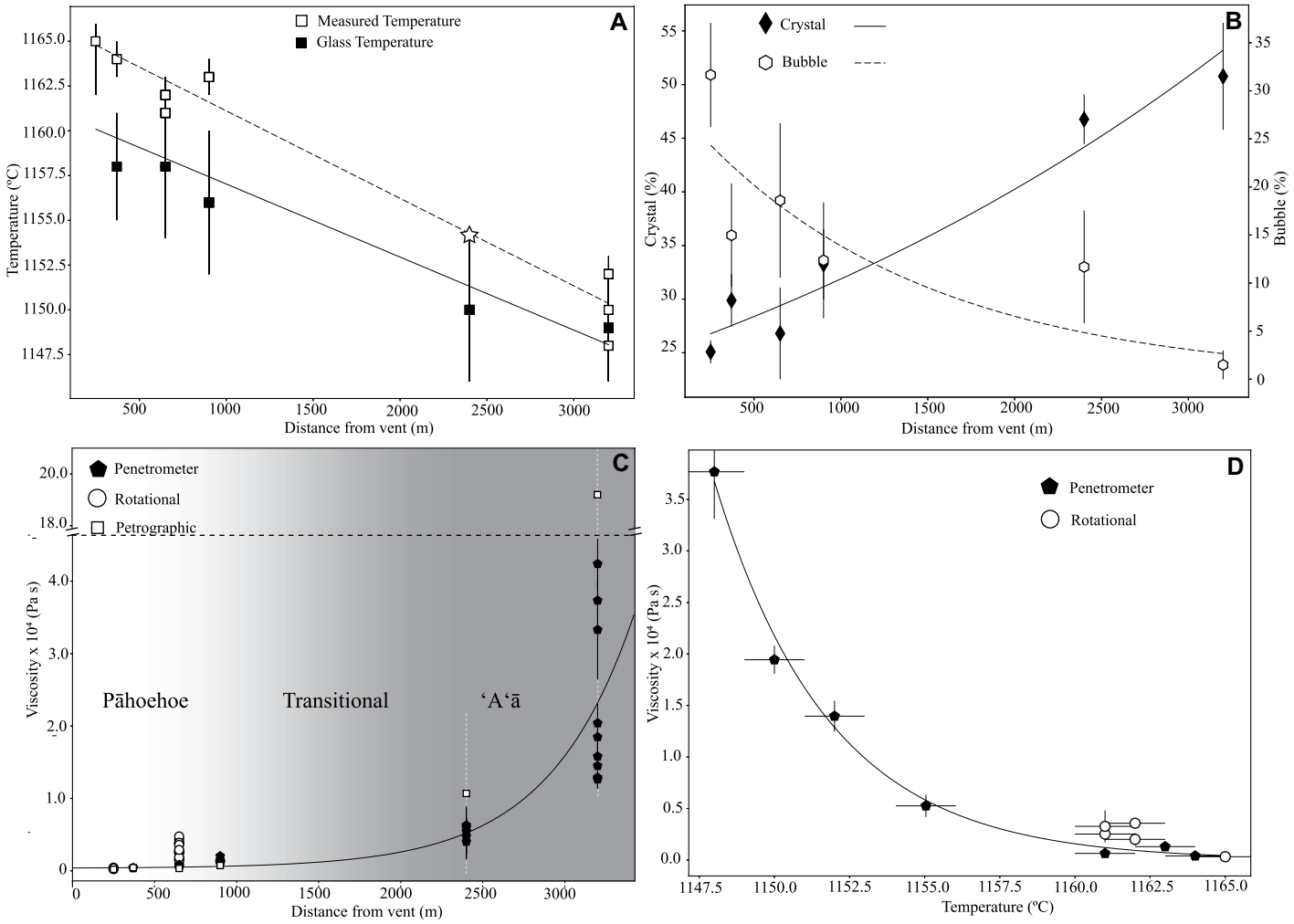

Figure 3. Variation of (A) temperature (°C), (B) texture, and (C) viscosity (Pa·s) vs. distance from vent (m), and (D) viscosity vs. temperature. Star in A is corrected temperature for site 5 (see Results). For textures (in B), groundmass crystal content (black diamond) (%) is plotted on left *y* axis, and vesicle content (white hexagon) (%) is on right *y* axis. Vertical bars represent variations for in situ viscosity (in C and D) and temperature (in A and D) measurements and calculated phase proportions (in B). In C, dashed lines show uncertainties for viscosity obtained from petrographic model (see Item S5 [text footnote 1]). Dashed horizontal line in C denotes change in *y*-axis values.

packing fraction and the near-complete bubble loss in the lava (vesicularity decrease from 12% to 2%). This suggests that rheological transition zones in three-phase suspensions may be narrower than those in two-phase suspensions due to the combined contributions of both phases. This may result in more abrupt changes in eruptive behavior than that predicted from the linear combination of two-phase models.

Our in situ data provide the first quantification of viscosity changes, and major drivers, during naturally flowing lava. While these exact viscosity values are specific to this eruption, these findings show that in situ techniques improve our understanding of multiphase lava rheology and can help to refine existing models that use weighted phase proportions of crystals and vesicles.

Implications for Eruptive Response Protocols

We documented the dynamic evolution of temperature, crystallinity, and vesicularity of an active lava flow field with distance from the vent and their respective effects on the lava's viscosity (Fig. 3). We compared our in situ data with commonly used three-phase petrographic approaches to deduce lava viscosity (Fig. 3C; Item S5). This petrographic approach shows a similar trend of viscosity increase with distance. However, as a result of the limitations of models prescribing a rigid maximum packing fraction (e.g., Maron and Pierce, 1956), the uncertainties associated with this approach become extremely large, and it drastically overestimates lava viscosity when the crystal fraction exceeds 50% (i.e., sites 5–6; Fig. 3C; Item S5). To deduce these values, we used in situ temperature measurements, which are not always available; a method using temperatures recovered via MgO glass thermometry would further increase the petrologically derived viscosities. Furthermore, the time scales required to return samples from the field, prepare thin sections, quantify all relevant textural parameters, and obtain melt compositions for this modeling are on the order of days. Additionally, assumptions on relevant strain rates are needed to estimate Ca.

In contrast, in situ viscosity measurements, as we performed here, can be conducted and processed within minutes and relayed in near-real-time to researchers who model lava runout as part of civil protection responses (Chevrel et al., 2022; Harris et al., 2019). Initiation and real-time adjustment of such models with these in situ field viscosity data can greatly increase their accuracy.

CONCLUSION

We present the first-ever comprehensive real-time, in situ viscosity map of active lava. We measured the viscosity increase along the flow and correlated it to the thermal and textural evolution of the lava. The data show that at high crystal contents, in situ viscosity measurements are significantly lower and more accurate and precise than values derived from available pet-

rologic approaches. This study highlights the benefits of field viscometry, which is both more precise and faster than data obtainable with other approaches. Since we provide the first data set that covers an entire flow, this study marks a starting point for the validation and refinement of experimental and numerical parameterizations of multiphase lava rheology through field viscometry. Additionally, we present the first in situ constraints on the viscosity range of the pāhoehoe–ʻaʻā transition of actively flowing lava. Finally, this in situ methodology can aid global communities because it provides a real-time assessment of lava viscosity that can be implemented into eruptive models used for civil protection.

ACKNOWLEDGMENTS

We thank the University of Iceland for its generous support during the field campaign. Funding was provided by the State University of New York at Buffalo Center for Geological and Climate Hazards, National Science Foundation (NSF) EAR RAPID award no. 2241489, and NSF EAR awards no. 2223098 and 2420723. This is contribution 664 from the French Government Laboratory of Excellence Initiative ClerVolc.

REFERENCES CITED

Belousov, A., and Belousova, M., 2018, Dynamics and viscosity of ʻaʻa and pahoehoe lava flows of the 2012–2013 eruption of Tolbachik volcano, Kamchatka (Russia): Bulletin of Volcanology, v. 80, 6, https://doi.org/10.1007/s00445-017-1180-2.

Cappello, A., Hérault, A., Bilotta, G., Ganci, G., and Del Negro, C., 2016, MAGFLOW: A physics-based model for the dynamics of lava-flow emplacement, *in* Harris, A.J.L., De Groeve. T., Garel, F., and Carn, S.A., eds., Detecting, Modelling and Responding to Effusive Eruptions: Geological Society, London, Special Publication 426, p. 357–373, https://doi.org/10.1144/SP426.16.

Cashman, K.V., Thornber, C., and Kauahikaua, J.P., 1999, Cooling and crystallization of lava in open channels, and the transition of pāhoehoe lava to ʻaʻā: Bulletin of Volcanology, v. 61, p. 306–323, https://doi.org/10.1007/s004450050299.

Chevrel, M.O., Harris, A.J.L., James, M.R., Calabrò, L., Gurioli, L., and Pinkerton, H., 2018a, The viscosity of pāhoehoe lava: In situ syn-eruptive measurements from Kilauea, Hawaii: Earth and Planetary Science Letters, v. 493, p. 161–171, https://doi.org/10.1016/j.epsl.2018.04.028.

Chevrel, M.O., Pinkerton, H., and Harris, A.J.L., 2019, Measuring the viscosity of lava in the field: A review: Earth-Science Reviews, v. 196, 102852, https://doi.org/10.1016/j.earscirev.2019.04.024.

Chevrel, M.O., Harris, A.J.L., Peltier, A., Villeneuve, N., Coppola, D., Gouhier, M., and Drenne, S., 2022, Volcanic crisis management supported by near real-time lava flow hazard assessment at Piton de la Fournaise, La Réunion: Volcanica, v. 5, p. 313–334, https://doi.org/10.30909/vol.05.02.313334.

Chevrel, M.O., Latchimy, T., Batier, L., Delpoux, R., Harris, M.A., and Kolzenburg, S., 2023, A new portable field rotational viscometer for high-temperature melts: The Review of Scientific Instruments, v. 94, 105116, https://doi.org/10.1063/5.0160247.

Costa, A., and Macedonio, G., 2005, Computational modeling of lava flows: A review, *in* Manga, M., and Ventura, G., eds., Kinematics and Dynamics of Lava Flows: Geological Society of America Special Paper 396, p. 209–218, https://doi.org/10.1130/0-8137-2396-5.209.

Costa, A., Caricchi, L., and Bagdassarov, N., 2009, A model for the rheology of particle-bearing suspensions and partially molten rocks: Geochemistry, Geophysics, Geosystems, v. 10, Q03010, https://doi.org/10.1029/2008GC002138.

Dietterich, H.R., Diefenbach, A.K., Soule, S.A., Zoeller, M.H., Patrick, M.P., Major, J.J., and Lundgren, P.R., 2021, Lava effusion rate evolution and erupted volume during the 2018 Kīlauea lower East Rift Zone eruption: Bulletin of Volcanology, v. 83, 25, https://doi.org/10.1007/s00445-021-01443-6.

Di Fiore, F., Vona, A., Kolzenburg, S., Mollo, S., and Romano, C., 2021, An extended rheological map of pāhoehoe–ʻaʻā transition: Journal of Geophysical Research: Solid Earth, v. 126, https://doi.org/10.1029/2021JB022035.

Fink, J.H., and Zimbelman, J., 1990, Longitudinal variations in rheological properties of lavas: Puu Oo basalt flows, Kilauea Volcano, Hawaii, *in* Fink, J.H., ed., Lava Flows and Domes: IAVCEI Proceedings in Volcanology Volume 2: Berlin, Springer, p. 157–173, https://doi.org/10.1007/978-3-642-74379-5_7.

Guilbaud, M.N., Self, S., Thordarson, T., and Blake, S., 2005, Morphology, surface structures, and emplacement of lavas produced by Laki, A.D. 1783–1784, *in* Manga, M., and Ventura, G., eds., Kinematics and Dynamics of Lava Flows: Geological Society of America Special Paper 396, p. 81–102, https://doi.org/10.1130/0-8137-2396-5.81.

Harris, A.J.L., and Rowland, S.K., 2001, Kinematic thermo-rheological model for lava cooling in a channel: Bulletin of Volcanology, v. 63, p. 20–44, https://doi.org/10.1007/s004450000120.

Harris, A.J.L., et al., 2019, Validation of an integrated satellite-data-driven response to an effusive crisis: The April-May 2018 eruption of Piton de la Fournaise: Annals of Geophysics, v. 61, VO230, https://doi.org/10.4401/ag-7972.

Harris, M.A., Kolzenburg, S., Sonder, I., and Chevrel, M.O., 2024, A new portable penetrometer for measuring the viscosity of active lava: The Review of Scientific Instruments, v. 95, 65103, https://doi.org/10.1063/5.0206776.

Hon, K., Gansecki, C., and Kauahikaua, J., 2003, The transition from ʻaʻā to pāhoehoe crust on flows emplaced during the Pu'u ʻŌʻō–Kūpaianaha eruption, *in* Heliker, C., Swanson, D.A., and Takahashi, T.J., eds., The Puʻu ʻŌʻō-Kūpaianaha Eruption of Kīlauea Volcano, Hawaiʻi: The First 20 Years: U.S. Geological Survey Professional Paper 1676, p. 89–103, https://pubs.usgs.gov/pp/pp1676/pp1676_05.pdf.

Hyman, D.M.R., Dietterich, H.R., and Patrick, M.R., 2022, Toward next-generation lava flow forecasting: Development of a fast, physics-based lava propagation model: Journal of Geophysical Research: Solid Earth, v. 127, https://doi.org/10.1029/2022JB024998.

James, M.R., Bagdassarov, N., Müller, K., and Pinkerton, H., 2004, Viscoelastic behaviour of basaltic lavas: Journal of Volcanology and Geothermal Research, v. 132, p. 99–113, https://doi.org/10.1016/S0377-0273(03)00340-8.

Keszthelyi, L., Thordarson, T., McEwen, A., Haack, H., Guilbaud, M.N., Self, S., and Rossi, M.J., 2004, Icelandic analogs to Martian flood lavas: Geochemistry, Geophysics, Geosystems, v. 5, Q11014, https://doi.org/10.1029/2004GC000758.

Kolzenburg, S., Chevrel, M.O., and Dingwell, D.B., 2022, Magma/suspension rheology: Reviews in Mineralogy and Geochemistry, v. 87, p. 639–720, https://doi.org/10.2138/rmg.2022.87.14.

Krmíček, L., Troll, V.R., Thordarson, T., Brabec, M., Moreland, W.M., and Maťo, A., 2023, The 2023 Litli-Hrútur eruption of the Fagradalsfjall Fires, SW-Iceland: Insights from trace element compositions of olivine: Czech Polar Reports, v. 13, p. 257–270, https://doi.org/10.5817/CPR2023-2-20.

Lev, E., and James, M.R., 2014, The influence of cross-sectional channel geometry on rheology and flux estimates for active lava flows: Bulletin of Volcanology, v. 76, 829, https://doi.org/10.1007/s00445-014-0829-3; correction available at https://doi.org/10.1007/s00445-020-1356-z.

Mader, H.M., Llewellin, E.W., and Mueller, S.P., 2013, The rheology of two-phase magmas: A review and analysis: Journal of Volcanology and Geothermal Research, v. 257, p. 135–158, https://doi.org/10.1016/j.jvolgeores.2013.02.014.

Maron, S.H., and Pierce, P.E., 1956, Application of Ree-Eyring generalized flow theory to suspensions of spherical particles: Journal of Colloid Science, v. 11, p. 80–95, https://doi.org/10.1016/0095-8522(56)90023-X.

Moore, H.J., 1987, Preliminary estimates of the rheological properties of 1984 Mauna Loa lava, *in* Decker, R.W., Wright, T.L., and Stauffer, P.H., eds., Volcanism in Hawaii: U.S. Geological Survey Professional Paper 1350, p. 1569–1588, https://pubs.usgs.gov/pp/1987/1350/pdf/chapters/pp1350_ch58.pdf.

Pankhurst, M.J., et al., 2022, Rapid response petrology for the opening eruptive phase of the 2021 Cumbre Vieja eruption, La Palma, Canary Islands: Volcanica, v. 5, p. 1–10, https://doi.org/10.30909/vol.05.01.0110.

Pinkerton, H., and Sparks, R.S.J., 1978, Field measurements of the rheology of lava: Nature, v. 276, p. 383–385, https://doi.org/10.1038/276383a0.

Robert, B., Harris, A., Gurioli, L., Médard, E., Sehlke, A., and Whittington, A., 2014, Textural and rheological evolution of basalt flowing down a lava channel: Bulletin of Volcanology, v. 76, 824, https://doi.org/10.1007/s00445-014-0824-8.

Thordarson, T., et al., 2023, The 2021, 2022, and 2023 eruptions of Fagradalsfjall Fires, Reykjanes Peninsula Iceland: San Francisco, California, America Geophysical Union, Fall Meeting, abstract V32A–02.

Wieser, P., Petrelli, M., Lubbers, J., Wieser, E., Ozaydin, S., Kent, A., and Till, C., 2022, Thermobar: An open-source Python3 tool for thermobarometry and hygrometry: Volcanica, v. 5, p. 349–384, https://doi.org/10.30909/vol.05.02.349384.

Printed in the USA